Biomaterials Science

ROYAL SOCIETY OF CHEMISTRY

PAPER

View Article Online
View Journal | View Issue

Check for updates

Cite this: *Biomater. Sci.*, 2025, **13**, 5390

Ultrasound-responsive azide nano-prodrugs enable spatiotemporal activation of TLR7/8 agonists for tumor therapy

Chuwen Luo,[a,b,c] Chaoying Kong,[a,b,c] Yuxiao Zhang,[d] Yajun Xu*[a,c] and Zhaohui Tang *[a,b,c]

Received 19th May 2025,
Accepted 14th August 2025

DOI: 10.1039/d5bm00755k

rsc.li/biomaterials-science

Systemic immunotoxicity caused by off-target activation is still a critical obstacle to clinical translation of imidazoquinoline (IMDQ) drugs, a kind of TLR7/8 agonist. Here, we present an ultrasound-responsive, azide-modified IMDQ nano-prodrug (IMDQ-N_3 NPs) that enables spatiotemporally controlled activation through ultrasound, improving the selectivity and safety. Concomitantly, riboflavin-based sonosensitizers were co-delivered to these nanoparticles, increasing their local concentration surrounding the prodrug, achieving a 12.2-fold enhancement in the ultrasonic reduction rate of IMDQ-N_3. In murine models, IMDQ-N_3 NPs demonstrated no weight loss and negligible systemic inflammatory factor elevation relative to equivalent-dose unmodified IMDQ. Combined with ultrasound irradiation, IMDQ-N_3 NPs demonstrated 35.2-fold higher tumor distribution of active drug compared to non-irradiated free IMDQ-N_3, achieving 95.7% tumor suppression and 60% long-term survival. Flow cytometry analysis revealed enhanced dendritic cell maturation, cytotoxic T-cell infiltration, and durable immune memory. This work establishes a generalizable platform for precision delivery of immunostimulatory agents, addressing key translational challenges in cancer immunotherapy.

1. Introduction

In recent years, immunotherapy has become one of the key directions of tumor treatment research.[1] In general, immunotherapy could hinder immune effector inhibition by enhancing the cancer-immunity cycle, thus strengthening the immune response to treat the cancer.[2] As the bridge between non-specific immunity and specific immunity, tumor antigen presentation is indispensable in most tumor immunotherapies.[3] Antigen presenting cells (APCs) are a class of immune cells that can uptake, process and present antigens. Among them, the function of activated dendritic cells (DCs) is the most potent.[4] As a consequence, the activation of DCs is significant.[5] Imidazoquinolines (IMDQs) are a kind of Toll-like receptor 7 and 8 (TLR7/8) agonist, which can bind to TLR7/8 on the endosomal membrane of immune cells to promote the release of type I interferon, proinflammatory cytokines and chemokines.[6] They can facilitate the activation of DCs, induce specific immunity of tumors and long-term immune memory.[7,8] Therefore, many IMDQ agonist drugs have successfully entered the clinic, for instance, imiquimod (R837), resiquimod (R848) and telratolimod.[9,10] However, due to their poor selectivity, IMDQs rapidly distribute throughout the body during therapy, leading to strong systemic immunotoxicity, including persistent fever, headache, or even a cytokine storm.[11,12] This has limited the therapeutic dose of IMDQs in the clinic, resulting in insufficient efficacy.[13] Consequently, reducing the toxicity of IMDQs without affecting their efficacy is the primary challenge to address currently.

Prodrug strategies are an effective approach to reduce side effects associated with drug therapy.[14] Most prodrugs are inactive precursors formed by covalent modification of active drugs. They can be converted to the active form by specific stimuli, increasing the concentration of active drugs at designated sites and reducing the systemic toxicity caused by off-target effects.[15,16] The research showed that the immune activation function of IMDQs depends on their amino structure, which is directly connected to their quinoline structure.[17,18] This is because the amino group can be recognized by forming hydrogen bonds with amino acid residues at the active site of

[a]*State Key Laboratory of Polymer Science and Technology, Changchun Institute of Applied Chemistry, Chinese Academy of Sciences, Changchun, Jilin, 130022, China. E-mail: ztang@ciac.ac.cn, yjxu@ciac.ac.cn*
[b]*School of Applied Chemistry and Engineering, University of Science and Technology of China, Hefei 230026, China*
[c]*Key Laboratory of Polymer Ecomaterials, Changchun Institute of Applied Chemistry, Chinese Academy of Sciences, Changchun, Jilin, 130022, China*
[d]*Department of Applied Biology and Chemical Technology, The Hong Kong Polytechnic University, Hong Kong 510640, China*

TLR7/8.[19] As a result, the modification of the amino group of IMDQs could significantly affect its biological activity, which could be used for preparing prodrugs to reduce the systemic immune-associated toxicity of IMDQs.[20]

Using ultrasound (US) to activate prodrugs is a kind of therapeutic approach with great potential in the field of tumor therapy.[21] US can induce the occurrence of sonochemical reactions.[22] Compared with other exogenous measures of activation, such as light, heat, radiation, and magnetic field, US has high penetration and safety. US can penetrate the barrier of the skin and tissue, directly reach the target, participate and regulate the process of drug release and transform *in vivo* without apparent side effects.[23] Unlike endogenous stimuli, such as pH, enzymes, hypoxia and so on, drug activation controlled by US has the advantages of precise spatiotemporal controllability and reduced impact from tumor heterogeneity.[24,25] Utilizing an ultrasonic activation strategy can effectively reduce the original toxicity of drugs and is a promising method for activating prodrugs.[26] Furthermore, US can induce local cell death in cancer and is an ideal supplementary measure for immunotherapy.[27] Consequently, US has great potential as a stimulus for the activation of IMDQ prodrugs. Organic azides are potential precursors for the preparation of amines through chemical reduction.[28] Due to the lack of hydrogen atoms, it is difficult for the azide group to form hydrogen bonds with the carbonyl group at the active site of TLR7/8, which will lead to a decrease in drug activity compared with the amino group.[19,20] At the same time, organic azides are relatively inert in normal tissues, and the only by-product of metabolic transformation into drugs is molecular nitrogen.[29] These advantages make azidation become an ideal strategy to prepare prodrugs for drugs that have amino groups as the active site. It has been reported that aromatic azides can be reduced to aromatic amines by radiation in water.[30] This includes a radical mediated reduction reaction, to be specific, the water molecules are split by radiation, releasing hydrogen radicals and reducing the azide group. In water, US can excite unstable bubbles through cavitation to create micro-reactors that can produce instantaneous high temperature and high pressure.[31] In this process, water molecules can be cleaved to produce hydrogen radicals as well.[32] Thus, it is possible for US to replace radiation in the reaction of reducing azides to amino groups. We verified this conjecture through treating azide modified IMDQ (IMDQ-N_3) by low intensity US with the help of sonosensitizers and reductants.

Based on the above theories, novel azide based IMDQ nanoprodrugs (IMDQ-N_3 NPs) are described in this study. The nano-prodrugs consisted of three parts, including poly(L-glutamic acid)-*graft*-methoxy poly(ethylene glycol) (PLG-*g*-mPEG), which served as the nanoparticle drug carrier, a side chain modified riboflavin (Rf-$(OH)_2$), which served as the sonosensitizer, and IMDQ-N_3, which served as the TLR7/8 agonist prodrug. These nanoparticles could be reduced by US at the tumor site to achieve a cancer selective therapy (Scheme 1). This design can utilize the enhanced permeability and retention effect of nanoparticles to prevent the active drug from wandering around and causing systemic toxicity, enhancing drug safety.[33,34] Simultaneously, US can enhance vascular permeability of the tumor, increasing the drug enrichment in the tumor, and improving the efficacy of drugs.[35] This work provides a feasible scheme for the development of immune-stimulatory drugs which has lower toxicity and higher efficiency, holding great prospects in tumor immunotherapy.

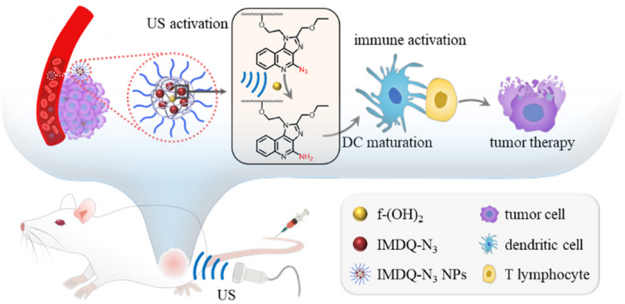

Scheme 1 Schematic diagram for the proposed antitumor mechanism of IMDQ-N_3 NPs.

2. Experimental procedures

2.1 Materials

4-Amino-2-ethoxymethyl-1*H*-imidazo[4,5-*c*]quinoline-1-ethanol (IMDQ) was purchased from Suzhou Norbeco Biotechnology Co., Ltd, China. The diazotizing species fluorosulfuryl azide (FSO_2N_3) was prepared according to a previous report.[36] Riboflavin (Rf) was purchased from Shanghai Yuanye Bio-Technology Co., Ltd, China. Sodium periodate ($NaIO_4$) was purchased from Shanghai Aladdin Biochemical Technology Co., Ltd, China. Poly(L-glutamic acid) (PLG) was synthesized according to our previous work.[37] *N*,*N*-Dimethylformamide (DMF) and 4-dimethylamino-pyridine (DMAP) were purchased from Anhui Senrise Technology Co., Ltd, China. 1-Ethyl-3-(3-dimethylaminopropyl)carbodiimide hydrochloride (EDC·HCl) was purchased from Bide Pharmatech Co., Ltd, China. Roswell Park Memorial Institute (RPMI) 1640 and phosphate-buffered saline (PBS) were purchased from Dalian Meilun Biotechnology Co., Ltd, China. Fetal bovine serum (FBS) was purchased from Zhejiang Tianhang Biotechnology Co., Ltd, China. All antibodies were purchased from BioLegend, Inc., America (Table S3). All other reagents and solvents were purchased from Sinopharm Chemical Reagent Co., Ltd, China and used as received.

2.2 Instrumentation for characterization

Proton nuclear magnetic resonance (^{1}H NMR) and carbon-13 nuclear magnetic resonance (^{13}C NMR) spectra were recorded on a Bruker AV 300 spectrometer at room temperature in trifluoroacetic acid-*d*, dimethyl sulfoxide-*d*6 or a sodium deuteroxide/deuterium oxide solution. Electrospray ionization mass spectroscopy (ESI-MS) was performed on a Bruker APEX-IV Fourier transform mass spectrometer. Dynamic laser scattering (DLS) measurement was performed on a Malvern Zetasizer

(Nano-ZS) instrument. A high-performance liquid chromatography (HPLC, EClassical 3100 System) system equipped with a reverse-phase column (Supersil ODS2) was used. Liquid chromatography-mass spectrometry (LC-MS) was performed on a Triple TOF 5600 mass spectrometer with an electrospray ionization source, Analyst TF data processing software, an Agilent 1100 liquid chromatography system, and a Shimadzu UFLC SIL 20A XR column compartment. Ultrasound-related experiments were conducted with a Chattanooga Intelect Mobile Ultrasound (2776).

2.3 Synthesis of IMDQ-N_3 and Rf-$(OH)_2$

IMDQ-N_3 was synthesized through the reaction of IMDQ with FSO_2N_3. Briefly, IMDQ solution (125.4 mg dissolved in 8.0 mL DMF), and potassium bicarbonate ($KHCO_3$) solution (336.0 mg $KHCO_3$ dissolved in 1.3 mL water) were added to the FSO_2N_3 solution (58.7 mg FSO_2N_3 dissolved in 8.0 mL methyl *tert*-butyl ether). The mixture was stirred overnight at room temperature. After the reaction, ethyl acetate (20.0 mL) and water (20.0 mL) were added to the mixture. The sediment was separated and purified by silica gel chromatography (dichloromethane/methanol 98 : 2) to obtain IMDQ-N_3 (98.1 mg, 71.8%).

Rf-$(OH)_2$ was synthesized by the reaction of Rf with $NaIO_4$. Briefly, Rf (1053.8 mg) and $NaIO_4$ (1796.7 mg) were dispersed in 40.0 mL water. The suspension was stirred overnight at room temperature away from light. The sediment was separated and sequentially washed with water (200.0 mL), methanol (200.0 mL) and ether (100.0 mL) to acquire Rf-$(OH)_2$ (698.3 mg, 82.5%).

2.4 Preparation of nanoparticles

IMDQ-N_3 NPs were synthesized by the esterification reaction of IMDQ-N_3, Rf-$(OH)_2$, and methoxy poly(ethylene glycol) (mPEG) with PLG. In brief, PLG solution (100.0 mg dissolved in 10.0 mL DMF), mPEG solution (100 mg dissolved in 5.0 mL DMF), EDC·HCl solution (185.9 mg dissolved in 10.0 mL DMF) and DMAP solution (113.6 mg dissolved in 3.0 mL DMF) were successively added to a 100 mL round-bottom flask under the protection of argon. The mixture was stirred at 40 °C for 4 h. The IMDQ-N_3 solution (31.4 mg dissolved in 2.0 mL DMF) and Rf-$(OH)_2$ solution (99.8 mg dissolved in 5.0 mL DMSO) were added to the reaction mixture every 4 h under the protection of argon, orderly. After 72 h, cold ether (175.0 mL) was added to the mixture, then the precipitate was collected and dissolved in 20.0 mL DMF after vacuum drying. Salting with sodium bicarbonate, dialysis in water, and then freeze-drying were carried out to get the product (171.6 mg).

Non-riboflavin-carrying IMDQ-N_3 NPs (NF IMDQ-N_3 NPs) were synthesized by the esterification reaction of IMDQ-N_3, methoxy poly(ethylene glycol) (mPEG) with PLG. In brief, the PLG solution (100.0 mg dissolved in 10.0 mL DMF), mPEG solution (100 mg dissolved in 5.0 mL DMF), EDC·HCl solution (183.7 mg dissolved in 10.0 mL DMF) and DMAP solution (109.2 mg dissolved in 3.0 mL DMF) were successively added to a 100 mL round-bottom flask under the protection of argon. The mixture was stirred at 40 °C for 4 h. IMDQ-N_3 solution (33.1 mg dissolved in 2.0 mL DMF) was added to the reaction mixture under the protection of argon. After 72 h, cold ether (175.0 mL) was added to the mixture, and then the precipitate was collected and dissolved in 20.0 mL DMF after vacuum drying. Salting with sodium bicarbonate, dialysis in water, then freeze-drying were carried out to get the product (142.1 mg).

The two kinds of macromolecules can form nanoparticles in aqueous solution *via* self-assembly.

2.5 *In vitro* ultrasonic reduction of IMDQ-N_3 NPs

IMDQ-N_3 NPs (1.0 μg mL^{-1}, calculated in the IMDQ-N_3 form) were dissolved in water. The samples were packed into closed containers sheltered from light, each containing 600.0 μL. US (1.0 MHz, 50% duty cycle, 5.0 min) treatment was performed at room temperature at power densities of 0.0 W cm^{-2}, 0.5 W cm^{-2}, 1.0 W cm^{-2}, 1.5 W cm^{-2}, 2.0 W cm^{-2} and 2.5 W cm^{-2}, to assess the effects of ultrasonic power density on reduction efficiency. Conversely, US (1.0 MHz, 2.0 W cm^{-2}, 50% duty cycle) was performed at room temperature for 0.0 min, 1.0 min, 2.0 min and 5.0 min, to evaluate the effects of ultrasonic duration on reduction efficiency. After US treatment, 10.0 μL of 1 M NaOH solution was added to hydrolyze IMDQ-N_3 NPs overnight. The pH of the solution was adjusted with phosphoric acid to about 9 and the sample was analysed by HPLC, using gradient elution to quantify, from methanol : H_2O (10 : 90, v/v) to pure methanol, for 23.0 min, at a flow rate of 1.0 mL min^{-1} and detected at 245 nm.

CT26 tumors (100.0 mm^3) were collected from CT26 tumor-bearing female BALB/c mice (6–8 weeks old) following oral administration of 20 μg Rf-$(OH)_2$ 1 h prior. Tumors were simply homogenized to prepare the tumor tissue homogenate. IMDQ-N_3 NPs and NF IMDQ-N_3 NPs (1.0 μg mL^{-1}, both calculated in the IMDQ-N_3 form) were respectively dissolved in the CT26 tumor homogenate. The samples were packed into closed containers sheltered from light, each containing 600.0 μL. US treatment (1.0 MHz, 2.0 W cm^{-2}, 50% duty cycle) was then performed at room temperature for 5.0 min. 10.0 μL of 1 M NaOH solution was added to hydrolyze overnight. The supernatant was separated, the pH was adjusted with phosphoric acid to about 9 and the sample was analysed by HPLC, using gradient elution to quantify, from methanol : H_2O (10 : 90, v/v) to pure methanol, for 23.0 min, at a flow rate of 1.0 mL min^{-1} and detected at 245 nm. The formation rates were calculated as follows: formation rate = C (IMDQ)/C (initial amount of IMDQ-N_3).

2.6 Cell culture and animals

Mouse colorectal cancer cells (CT26) were cultured in RPMI 1640 at 37 °C under a 5% CO_2 atmosphere. RPMI 1640 supplemented with 10% FBS, 50 U mL^{-1} penicillin and 50 U mL^{-1} streptomycin was used.

Female BALB/c mice (4–6 weeks old) were obtained from Beijing Vital River Laboratory Animal Technology Co., Ltd, China. C57BL/6N mice (4–5 weeks old) and Sprague Dawley (SD) rats were obtained from Jilin Qianhe Model

Biotechnology Co., Ltd, China. All animals received care in compliance with the guidelines outlined in the Guide for the Care and Use of Laboratory Animals. CT26 tumor-bearing mouse models were established by injecting 1.0×10^6 CT26 cells subcutaneously into the right back of each mouse. All animal procedures were performed in accordance with the Guidelines for Care and Use of Laboratory Animals of Changchun Institute of Applied Chemistry, Chinese Academy of Sciences and approved by the Animal Ethics Committee of Changchun Institute of Applied Chemistry, Chinese Academy of Sciences (CIAC 2023-0137).

2.7 *In vitro* drug activity analysis

Bone marrow-derived dendritic cells (BMDCs) were collected through the femurs and tibias of female BALB/c mice (6–8 weeks old), and cultured in the presence of IL-4 (10.0 ng mL^{-1}) and GM-CSF (20.0 ng mL^{-1}) for 7 days. After that, BMDCs were divided into 6 groups (3×10^5 cells per group): PBS with or without US (1.0 MHz, 2.0 W cm^{-2}, 50% duty cycle, 2.0 min), IMDQ (10.0 μg mL^{-1}) with or without US (1.0 MHz, 2.0 W cm^{-2}, 50% duty cycle, 2.0 min) and IMDQ-N_3 NPs (10.0 μg mL^{-1}, calculated in IMDQ form) with or without US (1.0 MHz, 2.0 W cm^{-2}, 50% duty cycle, 2.0 min), and cultured in 2.0 mL RPMI 1640 medium with the drugs mentioned above for 24 h. Then, BMDCs were collected and stained with anti-CD11c-FITC, anti-CD80-APC and anti-MHCII-APC/Cy7 antibodies. The activation of DCs was detected by flow cytometry.

2.8 *In vitro* analysis of bonding stability of IMDQ-N_3 NPs

1.0 mL IMDQ-N_3 NPs (0.5 mg mL^{-1}, calculated in IMDQ-N_3 form) were put inside a dialysis tubing (5 kDa), and 49.0 mL PBS (pH = 7.4 or 6.8) was added outside at 4 °C or 37 °C. 1.0 mL PBS outside the dialysis tubing was collected at 1, 2, 4, 8, 12, 24, 36, 48, 72 and 96 h, and the concentration of free IMDQ-N_3 was determined by HPLC, eluted with acetonitrile : water (50 : 50, v/v), at a flow rate of 1.0 mL min^{-1} and detected at 245 nm. The outside solution was replenished with 49.0 mL with PBS before each collection. The cumulative release ratios were calculated as follows: cumulative release ratios = C (total amount of free drugs)/C (initial amount of drugs inside dialysis tubing).

2.9 *In vitro* and *in vivo* toxicity analysis

The CCK-8 assay was performed to evaluate the *in vitro* cytotoxicity of IMDQ and IMDQ-N_3 NPs against CT26 tumor cells. Specifically, CT26 tumor cells (5×10^3 cells, in 180 μL RPMI 1640) were added to each well of the 96-well plates and cultured overnight at 37 °C with 5% CO_2. Then, IMDQ or IMDQ-N_3 NPs were added at final concentrations of 0, 10.0, 30.0, and 50.0 μg mL^{-1} (calculated in the IMDQ form, each group in triplicate) and incubated for 24 h. After incubation, 20 μL CCK-8 solution was added to each well and the cells were cultured for 2 h. Absorbance was measured at 450 nm to determine cell viability.

Female BALB/c mice (6–8 weeks old) were divided into 7 groups (n = 3), including a blank control group treated with PBS, three control groups treated with different concentrations of IMDQ (10.0 mg kg^{-1}, 30.0 mg kg^{-1} and 50.0 mg kg^{-1}) and three experimental groups treated with different concentrations of IMDQ-N_3 NPs (10.0 mg kg^{-1}, 30.0 mg kg^{-1} and 50.0 mg kg^{-1}, calculated in IMDQ form). Drugs were administered through the tail vein. The weights and survival rates of mice were measured within six days after administration. Another 21 female BALB/c mice (6–8 weeks old) and 21 CT26 tumor-bearing female BALB/c mice (6–8 weeks old) with the average volume of tumor of approximately 100.0 mm^3 were divided according to the same method (n = 3), and their serum samples were collected 6 h after treatment (through centrifugation, 3000 rpm, at 4 °C for 10.0 min). The levels of IL-6, TNF-α in the serum were detected by ELISA according to the manufacturer's instructions.

2.10 *In vivo* pharmacokinetic study

Female SD rats (average weight 200 g) were used to study the pharmacokinetics of two kinds of drugs (n = 3): free IMDQ-N_3 (10 mg kg^{-1}) and IMDQ-N_3 NPs (10.0 mg kg^{-1}, calculated in the IMDQ-N_3 form). The drugs were administered through the tail vein, and the serum was obtained through centrifugation of whole blood collected by capillary from the orbital cavity at each time point (5 min, 1 h, 2 h, 4 h, 8 h, 12 h, 24 h, 36 h, 48 h, and 96 h). The pH of serum was adjusted to 13 for hydrolyzing the drug overnight. The pH of the obtained supernatant was adjusted to 9 and the sample was analyzed by HPLC, eluted with acetonitrile : H_2O (v/v, 40 : 60) and detected at 245 nm at a flow rate of 1.0 mL min^{-1}. The half-life of the drug ($t_{1/2}$) was obtained by logarithmic fitting of the relationship between the drug concentration and time.

2.11 *In vivo* biodistribution

Female CT26 BALB/c tumor-bearing mice (6–8 weeks old) with the average tumor volume of approximately 100.0 mm^3 were divided into 2 time points (4.0 h and 12.0 h) and 4 material groups (n = 3): free IMDQ-N_3 (10.0 mg kg^{-1}) with or without US (1.0 MHz, 2.0 W cm^{-2}, 50% duty cycle, 2.0 min) and IMDQ-N_3 NPs (10.0 mg kg^{-1}, calculated in the IMDQ-N_3 form) with or without US (1.0 MHz, 2.0 W cm^{-2}, 50% duty cycle, 2.0 min). Mice were euthanized at the selected time point, their organs and tumors were collected, accurately weighed and homogenized with acetonitrile : H_2O (v/v, 50 : 50). The mixture was centrifuged, the supernatant was separated and sodium hydroxide was added to adjust the pH to about 13. The mixture was left at room temperature overnight until the nanoparticles completely dissociated, and the pH of the supernatant was adjusted to about 9 with phosphoric acid. The biodistribution of active IMDQ and total IMDQ (including nonactivated prodrugs, IMDQ-N_3) was measured by HPLC eluted with acetonitrile : H_2O (v/v, 30 : 70), detected at 250 nm (IMDQ) and 245 nm (IMDQ-N_3) at a flow rate of 1.0 mL min^{-1}.

2.12 Antitumor efficacy

Female CT26 BALB/c tumor-bearing mice (6–8 weeks old) with the average tumor volume approximately 100.0 mm^3 were used

to evaluate the antitumor efficiency of IMDQ-N_3 NPs activated by US. They were divided into six groups (n = 5), including two PBS injection group, with or without US (1.0 MHz, 2.0 W cm^{-2}, 50% duty cycle, 2.0 min). Four IMDQ-N_3 NP injection groups (10.0 mg kg^{-1} or 30.0 mg kg^{-1}, calculated in IMDQ form), with or without US (1.0 MHz, 2.0 W cm^{-2}, 50% duty cycle, 2.0 min). Mice in each group were administered through the tail vein as shown above on day 0, 2, and 4, respectively. Antitumor efficacy was evaluated through measuring tumor volume using vernier calipers every two days. Mice body weight was also measured to assess the toxicity of drugs. The tumor volume (V) was calculated as follows: V = a (the major axis length of the tumor) × b (the minor axis length of the tumor)^2/2. The tumor suppression rate (TSR) was calculated as follows: TSR (%) = [V_c (the average tumor volume of the PBS group) − V_x (the average tumor volume of the treatment group)]/V_c × 100%. The Q value was calculated using the following equation: Q = TSR (IMDQ-N_3 NPs + US)/[TSR (IMDQ-N_3 NPs) + TSR (US) − TSR (IMDQ-N_3 NPs) × TSR (US)]. $Q < 0.85$, $0.85 \leq Q < 1.15$, $Q \geq 1.15$ represent the antagonistic, additive and synergistic effects between the two therapeutic approaches, respectively.

Mice were euthanized on the tenth day after treatment. All tumors were isolated and photographed. Major organs and tumors of one mouse in each group were collected and fixed with paraformaldehyde buffered by 4% (W/V) PBS for 48 h, then embedded in paraffin, cut into 5 μm thick slices and stained with hematoxylin and eosin (H&E). Other tumor slices were stained with anti-CD8 antibodies to detect the infiltration of $CD8^+$ T cells in tumors. The other four tumors and spleens were analyzed by flow cytometry. Tumors were digested in a tumor dissociation buffer and filtered through nylon mesh to get single-cell suspensions. Spleens were mechanically separated, resuspended in RPMI 1640 and filtered through nylon mesh to get single-cell suspensions. Tumor single-cell suspensions were stained with anti-CD3-FITC, anti-CD4-PE/Cy7, and anti-CD8-APC antibodies for T cells; anti-CD11c-PE, anti-CD80-APC and anti-MHCII-PE/Cy7 antibodies for activated DCs; anti-CD11b-FITC, anti-F4/80-PE/Cy7 and anti-CD80-APC antibodies for M1 macrophages. Spleen single-cell suspensions were stained with anti-CD3-FITC, anti-CD4-PE/Cy7, anti-CD8-APC and anti-CD44-PE antibodies for T cells and memory T cells. This percentage reflects the ratio of specific immune cells to the total number of living cells. Population gating of the initial cell population was performed using only FSC and SSC maps of the cell samples. The gating strategy for all samples was set to remove cell debris, dead cells and large clumps or aggregates of cells.

Whole blood samples were collected from the treated mice mentioned above for centrifugation (3000 rpm, at 4 °C for 10.0 min) to separate serum. The levels of IL-6, TNF-α and IFN-γ in the serum were detected by ELISA according to the manufacturer's instructions. Furthermore, serum samples were also used for biochemical function analysis. Serum levels of alkaline phosphatase (AKP), aspartate aminotransferase (AST) and alanine aminotransferase (ALT) were measured to evaluate liver function, and serum levels of blood urea nitrogen (BUN), creatinine (CRE) and uric acid (UA) were measured to evaluate kidney function.

2.13 Statistical analysis

All quantitative data were analyzed in GraphPad and expressed as the mean ± SEM. Multigroup comparisons employed one-way analysis of variance (ANOVA) followed by Tukey's Honestly Significant Difference test. Significance was considered at $P < 0.05$. (*$P < 0.05$, **$P < 0.01$, ***$P < 0.001$ and ****$P < 0.0001$).

3. Results and discussion

3.1 Characterization of IMDQ-N_3 NPs

IMDQ-N_3 NPs were prepared through the esterification reaction, to be more specific, IMDQ-N_3.[36] (Fig. S1), 10-(2,2-dihydroxylethyl)-7,8-dimethylisoalloxazine (Rf-$(OH)_2$) (Fig. S2A) and methoxy poly(ethylene glycol) (mPEG) were bonded to the poly (L-glutamic acid) (PLG)[37] (Fig. S2B) by ester bonds (Fig. 1A). Ultraviolet–visible spectra indicated that IMDQ-N_3 was successfully loaded on the nanoparticles (Fig. 2A). The structure of IMDQ-N_3 NPs was verified by the ^{1}H NMR spectrum (Fig. 1B), and the drug loading content was measured as 8.2 wt% and 1.0 wt% by high performance liquid chromatography (HPLC) for IMDQ-N_3 and Rf-$(OH)_2$ (Fig. 1C). The particle size and surface charge of nanoparticles can affect their interactions with microvessels and stroma of tumor, ultimately affecting the drug enrichment in tumors.[38] Next, the particle size and surface charge were measured by dynamic laser scattering (DLS) and zeta-potential analysis. The particle size of IMDQ-N_3 NPs in water was 81.5 nm, with a polydispersity index (PDI) of 0.263 (Fig. 1D). The surface charge of IMDQ-N_3 NPs was −3.3 ± 0.8 mV (Fig. 1E). The negative charge reduces the cellular uptake of nanoparticles and improves their cycling capacity.[39] The particle size of IMDQ-N_3 NPs could be maintained for 7 days in PBS with or without 10% serum at 4 °C, indicating good particle size stability of IMDQ-N_3 NPs (Fig. 1F).

In order to reduce the systemic toxicity of IMDQ, it is most important to reduce the free drug content in non-targeted tissues. Drug bond stability tests *in vitro* has shown that the bonding of IMDQ-N_3 with nanoparticles was stabilized both in cold storage (4 °C) (Fig. 2B) or body temperature (37 °C) (Fig. 2C) at pH 7.4 or 6.8 in PBS. Pharmacokinetic analysis has shown that the average half-life of IMDQ-N_3 NPs was 8.6 times longer than that of free IMDQ-N_3 (Fig. S3), indicating good bioavailability of IMDQ-N_3.

3.2 US reduction of IMDQ-N_3 NPs *in vitro*

To verify the ultrasonic responsiveness of azide, we subjected IMDQ-N_3 NPs aqueous solution to US (1.0 MHz, 50% duty cycle, 5.0 min) at different ultrasonic power densities. The results showed that ultrasonic power density of 2.0 W cm^{-2} was optimal (Fig. S4A). Then, we subjected IMDQ-N_3 NPs aqueous solution to US (1.0 MHz, 2.0 W cm^{-2}, 50% duty cycle) for different time lengths. The results were evaluated by HPLC (Fig. 2D). IMDQ-N_3 NPs have shown good reducibility under US. In detail, compared with no US conditions, after 5.0 min

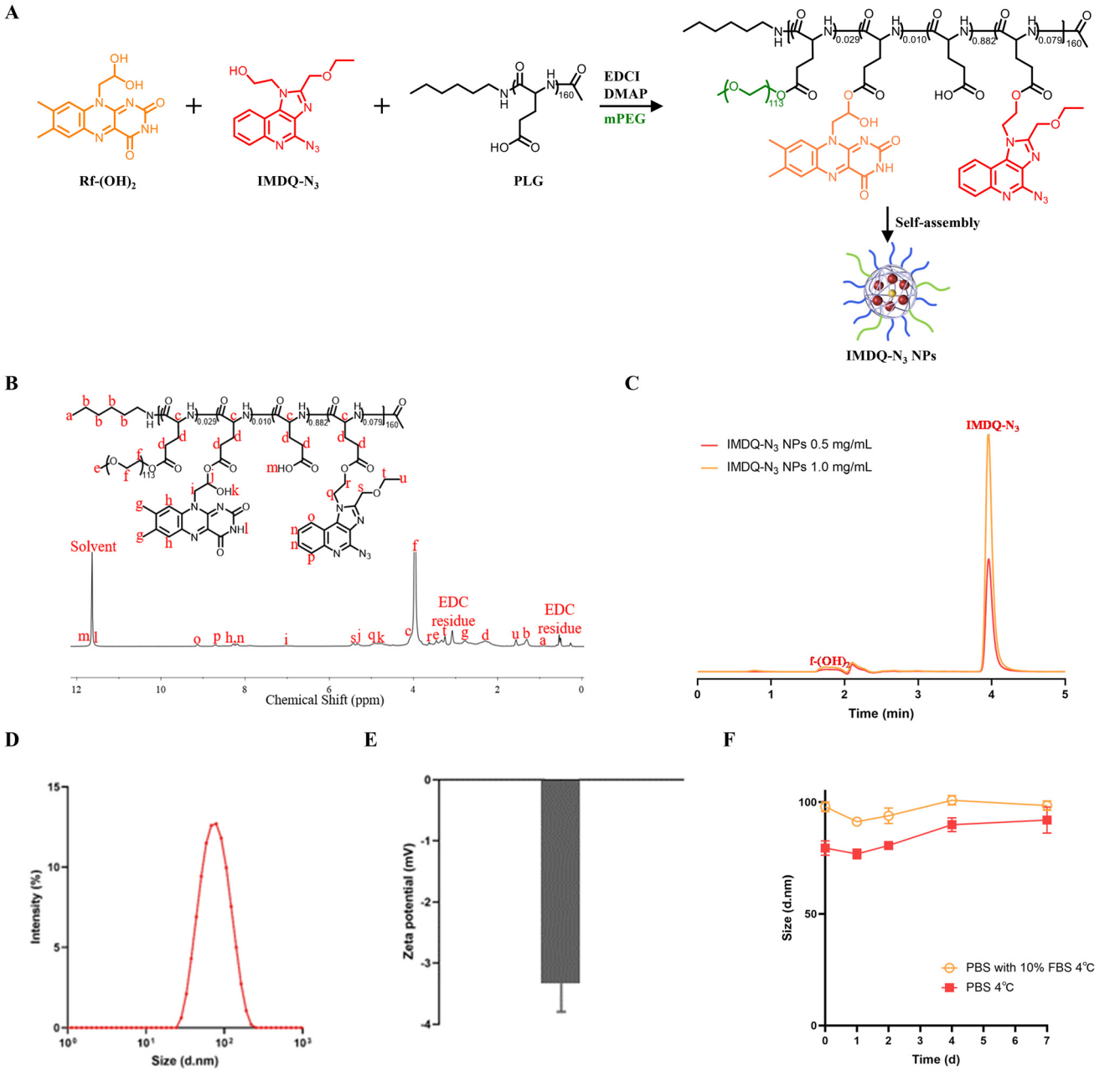

Fig. 1 Synthesis and characterization of IMDQ-N_3 NPs. (A) Synthesis route of IMDQ-N_3 NPs. (B) ^{1}H NMR spectrum of IMDQ-N_3 NPs in TFA-*d*. (C) Alkaline hydrolysis result of IMDQ-N_3 NPs by HPLC, acetonitrile : H_2O (60 : 40, v/v) at 245 nm. (D) Hydrodynamic diameter distribution of IMDQ-N_3 NPs in aqueous solution by DLS. (E) Surface potential of IMDQ-N_3 NPs in aqueous solution (n = 3). (F) Particle size stability of IMDQ-N_3 NPs in PBS with or without fetal bovine serum (FBS). Results are expressed as mean ± SEM (n = 3).

of US, the formation rates of IMDQ were about 9.95% (Table S1, SI). The types of reduction products were identified by liquid chromatography-mass spectrometry (LC-MS) and confirmed to be IMDQ (Fig. S4B). This result indicated that US reduced the azide groups to amines.

To validate the essential role of the sonosensitizer loaded in nanoparticles, a non-riboflavin-conjugated nano-prodrug, NF IMDQ-N_3 NP, was synthesized as a control. Since endogenous riboflavin exists *in vivo*, both IMDQ-N_3 NPs and NF IMDQ-N_3 NPs were dissolved in CT26 tumor homogenate derived from tumor-bearing female BALB/c mice pre-treated with oral excessive Rf-$(OH)_2$. Both groups were then irradiated by US (1.0 MHz, 2.0 W cm^{-2}, 50% duty cycle, 5.0 min). HPLC analysis (Fig. 2E) revealed a 12.2-fold higher formation rate of IMDQ in IMDQ-N_3 NPs (13.7%) compared with the control group NF IMDQ-N_3 NPs (1.1%). These results demonstrate that the riboflavin in the nanoparticles was necessary for ultrasonic reduction of IMDQ-N_3 NPs.

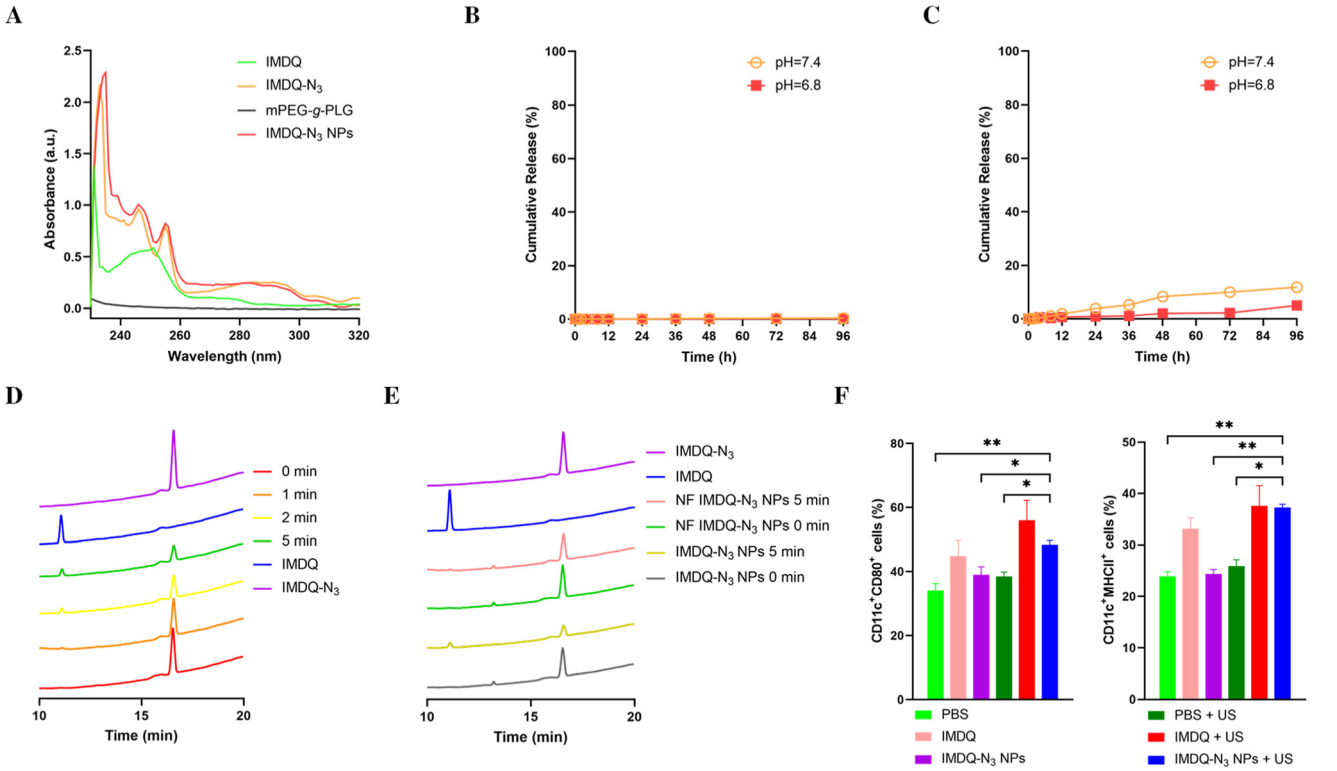

Fig. 2 The physical and chemical properties of IMDQ-N_3 NPs. (A) Ultraviolet–visible spectra of IMDQ-N_3 NPs and all their components, including a comparison with no azide-modified IMDQ. (B) IMDQ-N_3 release of IMDQ-N_3 NPs at pH 7.4 or 6.8 in PBS under refrigerated conditions (4 °C) (n = 3). (C) IMDQ-N_3 release of IMDQ-N_3 NPs at pH 7.4 or 6.8 in PBS at body temperature (37 °C) (n = 3). (D) Chemical reduction of IMDQ-N_3 NPs under US (1.0 MHz, 2.0 W cm^{-2}, 50% duty cycle) by HPLC (gradient elution, from methanol : H_2O (10 : 90, v/v) to pure methanol, 23.0 min). (E) Chemical reduction of IMDQ-N_3 NPs and NF IMDQ-N_3 NPs under US (1.0 MHz, 2.0 W cm^{-2}, 50% duty cycle) by HPLC (gradient elution, from methanol : H_2O (10 : 90, v/v) to pure methanol, 23.0 min). (F) Flow cytometry analysis of DC activation. The above results are expressed as mean ± SEM (n = 3). P values were determined by one-way analysis of variance (ANOVA) followed by Tukey's Honestly Significant Difference test (ns, no significant difference, *P < 0.05, **P < 0.01, ***P < 0.001 and ****P < 0.0001).

The immunostimulative effect of IMDQ-N_3 NPs on APCs was also studied *in vitro* in the presence of US. Bone marrow derived DCs, extracted from C57BL/6N mice, were treated with the same drug concentration of IMDQ or IMDQ-N_3 NPs. The drug activity was determined by the proportion of mature DCs, to be specific, it was measured by flow cytometry through the expression of the surface markers of mature DCs ($CD11c^+CD80^+$ and $CD11c^+MHCII^+$) 24 h after administration (Fig. 2F). Under the treatment of IMDQ-N_3 NPs activated by US, the $CD11c^+CD80^+$ and $CD11c^+MHCII^+$ DCs were up-regulated to 48.3% and 37.3% on average, respectively, and the results were significantly higher than the PBS, PBS with US and IMDQ-N_3 NPs without US groups (Fig. S5), suggesting the effective activation of DCs. Compared to the IMDQ and IMDQ with the US group, there was a small decrease in the activity of the active nanomedical group with no significant difference, which was within the acceptable range. These results verified that IMDQ-N_3 NPs could be reduced by US and preserved the effect of the immunomodulator *in vitro*.

3.3 Toxicity analysis of IMDQ-N_3 NPs *in vivo*

In order to evaluate the systemic toxicity reducing effect of IMDQ-N_3 NPs compared to IMDQ, the body weight and the number of inflammatory cytokines in serum, including interleukin-6 (IL-6) and interferon-γ (IFN-γ) were measured after administration in mice. In brief, IMDQ and IMDQ-N_3 NPs were injected into Balb/C mice at a concentration of 10.0 mg kg^{-1} to 50.0 mg kg^{-1}. The results showed that the weight of mice in all groups decreased after IMDQ administration, with the maximum average weight loss of 9.9% in the 50.0 mg kg^{-1} group of IMDQ. The weight of mice continued to increase in all concentration groups after IMDQ-N_3 NPs administration (Fig. 3A). Besides, compared with the PBS group, IMDQ caused a significant increase in the serum levels of IL-6 and IFN-γ both in healthy mice (maximum 10.7-fold and 114.5-fold, respectively) and CT26 tumor bearing mice (maximum 13.8-fold and 19.6-fold, respectively). In contrast, the levels of IL-6 and IFN-γ in the serum barely increased both in healthy mice (maximum 1.3-fold and 3.3-fold, respectively) (Fig. 3B) and CT26 tumor bearing mice (maximum 1.7-fold and 2.1-fold, respectively) (Fig. 3C) after IMDQ-N_3 NP administration, compared with the PBS group. Thus, IMDQ-N_3 NPs significantly reduced the level of proinflammatory cytokines when treating mice with the same dose of IMDQ. A 10 mg kg^{-1} dose of IMDQ-N_3 was also injected into healthy Balb/C mice, causing no significant increase in the serum levels of IFN-γ (Fig. S6A)

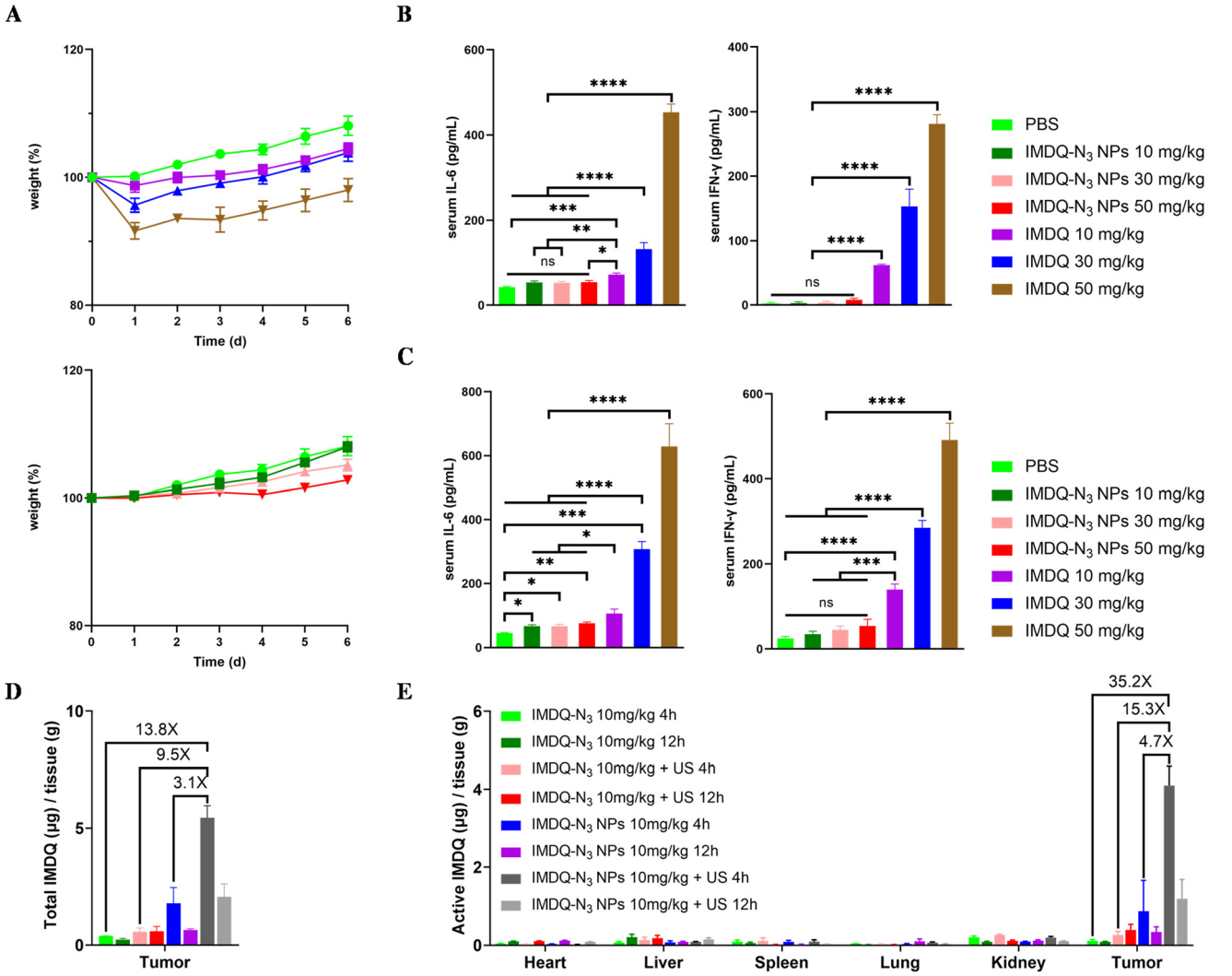

Fig. 3 The safety evaluation of IMDQ-N_3 NPs *in vitro* and the ultrasonic responsiveness evaluation of IMDQ-N_3 NPs *in vivo*. (A) Body weight percent of Balb/c mice after IMDQ or IMDQ-N_3 NP administration (n = 3). (B) Serum levels of IL-6 and IFN-γ in Balb/c mice 6 h after IMDQ or IMDQ-N_3 NP administration (n = 3). (C) Serum levels of IL-6 and IFN-γ in CT26 tumor bearing Balb/c mice 6 h after IMDQ or IMDQ-N_3 NP administration (n = 3). (D) Biodistribution of the total amount of IMDQ in tumors of CT26 tumor bearing Balb/c mice (n = 3). (E) Biodistribution of active IMDQ in CT26 tumor bearing Balb/c mice (n = 3). Results above are expressed as mean ± SEM P values were determined by one-way analysis of variance (ANOVA) followed by Tukey's Honestly Significant Difference test (ns, no significant difference, $^*P < 0.05$, $^{**}P < 0.01$, $^{***}P < 0.001$ and $^{****}P < 0.0001$).

and IL-6 (Fig. S6B) in healthy mice. Due to its low solubility in PBS (even with 50% cosolvent), it was impossible to compare the toxicity of free IMDQ-N_3 at higher doses in mice. Cytotoxicity of IMDQ and IMDQ-N_3 NPs was also measured (Fig. S6C), showing no significant cytotoxicity. These results demonstrated that IMDQ-N_3 NPs had a huge advantage in avoiding the side effects caused by systemic inflammation.

3.4 Biodistribution of IMDQ-N_3 NPs *in vivo*

The ultrasonic reduction of IMDQ-N_3 NPs *in vivo* was evaluated by their biodistribution in CT26 tumor bearing mice following intravenous administration of IMDQ-N_3 NPs at a concentration of 10.0 mg kg^{-1}. The US condition was applied under parameters identical to *in vitro* conditions, with the exposure duration reduced to 2.0 min to ensure the safety of mice. The results showed that the concentrations of active IMDQ and total IMDQ (including nonactivated prodrugs) in IMDQ-N_3 NPs with the US group were much higher than in other groups. To be specific, at 4 h post-injection, the concentration of total IMDQ in tumors was 13.8-fold higher than that in the free IMDQ-N_3 group, 9.5-fold greater than that in free IMDQ-N_3 with US group and 3.1-fold higher than the IMDQ-N_3 NPs group (Fig. 3D). The concentration of total IMDQ in all organs is shown in Fig. S7A. More strikingly, activated IMDQ concentrations demonstrated even more pronounced differences, with the US-treated IMDQ-N_3 NP group showing 35.2-fold, 15.3-fold, and 4.7-fold increases compared to the aforementioned control groups, respectively (Fig. 3E). The biodistribution of total IMDQ (Fig. S7B) and active IMDQ (Fig. S7C) in CT26 tumor bearing Balb/c mice at 24 h was also detected.

The distinction of drug concentration in the tumor between the control groups and the experimental group might be caused by the osmotic effect of US. Notably, the US-activated IMDQ-N_3 NPs exhibited exceptional tumor selectivity, with tumor-to-normal organ ratios reaching 196.3 : 1 (heart), 45.9 : 1 (liver), 43.5 : 1 (spleen), 57.0 : 1 (lungs), and 20.6 : 1 (kidneys) for activated IMDQ (Table S2, SI). Those results revealed that IMDQ-N_3 NPs had good tumor targeting ability and ultrasonic selective reduction ability *in vivo*.

3.5 Antitumor efficacy of IMDQ-N_3 NPs *in vivo*

After verifying the US reducing ability of IMDQ-N_3 NPs, we further evaluated their antitumor efficacy *in vivo* upon US activation. In this experiment, CT26 tumor bearing mice were treated with PBS, varying concentrations of IMDQ-N_3 NPs, and their combination with US. The therapeutic schedule is shown in Fig. 4A. The experiment was ceased on the 10th day when the average of tumor volume in the PBS group exceeded 1500.0 mm^3 (Fig. 4B). At this time point, the tumor suppression rate of the IMDQ-N_3 NPs (10.0 mg kg^{-1} and 30.0 mg kg^{-1}) combined with US treated groups were 86.2% and 95.7% compared with the control group, respectively, which were much higher than that of US only and IMDQ-N_3 NPs (10.0 mg kg^{-1} and 30.0 mg kg^{-1}) only groups, which were 15.7%, 45.9% and 61.6% compared with the control group, respectively (Fig. 4C). The synergy between IMDQ-N_3 NPs and US was evaluated by the Q value method and the calculated results were 1.59 (10.0 mg kg^{-1}) and 1.41 (30.0 mg kg^{-1}), suggesting that the therapeutic effects of IMDQ-N_3 NPs and US were not simply additive, which was in line with expectations. These results showed that US-activated IMDQ-N_3 NPs could significantly inhibit the growth of the tumor.

To assess the toxicity of IMDQ-N_3 NPs, body weight changes and inflammatory cytokine levels in the serum were measured

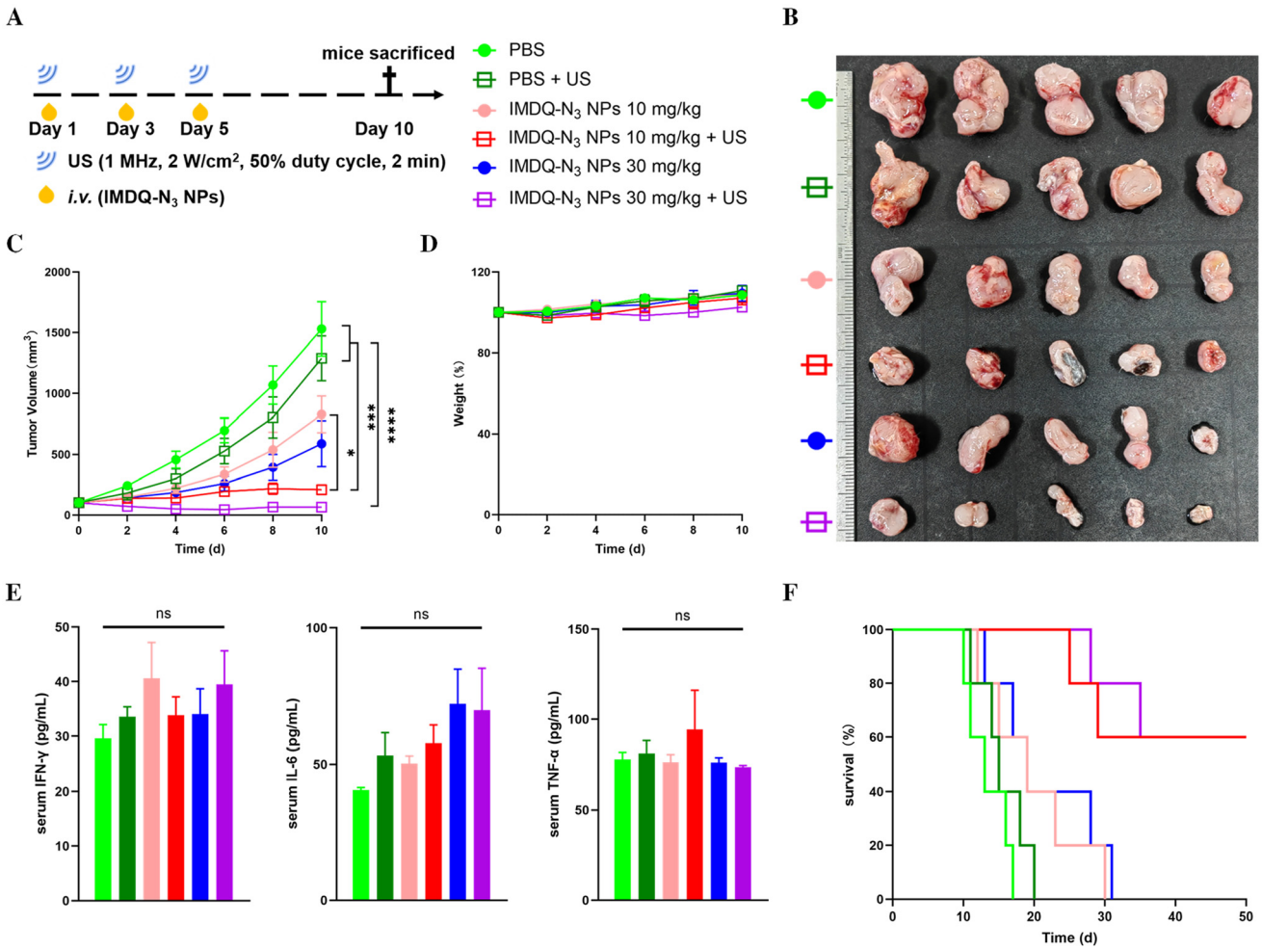

Fig. 4 Evaluation of tumor inhibition effect and safety of IMDQ-N_3 NPs *in vivo*. (A) The scheme used in the treatment. (B) Images of the excised tumor following 10 days of treatment in each group. (C) The tumor volume growth curve in each group. (D) The body weight variation in each group. (E) Serum levels of IFN-γ, IL-6 and TNF-α after treatment in each group. Serum levels of inflammatory cytokines. Results above are expressed as mean ± SEM (n = 5). (F) The survival rates of mice after treatment in each group (n = 5). P values were determined by one-way analysis of variance (ANOVA) followed by Tukey's Honestly Significant Difference test (ns, no significant difference, *P < 0.05, **P < 0.01, ***P < 0.001 and ****P < 0.0001).

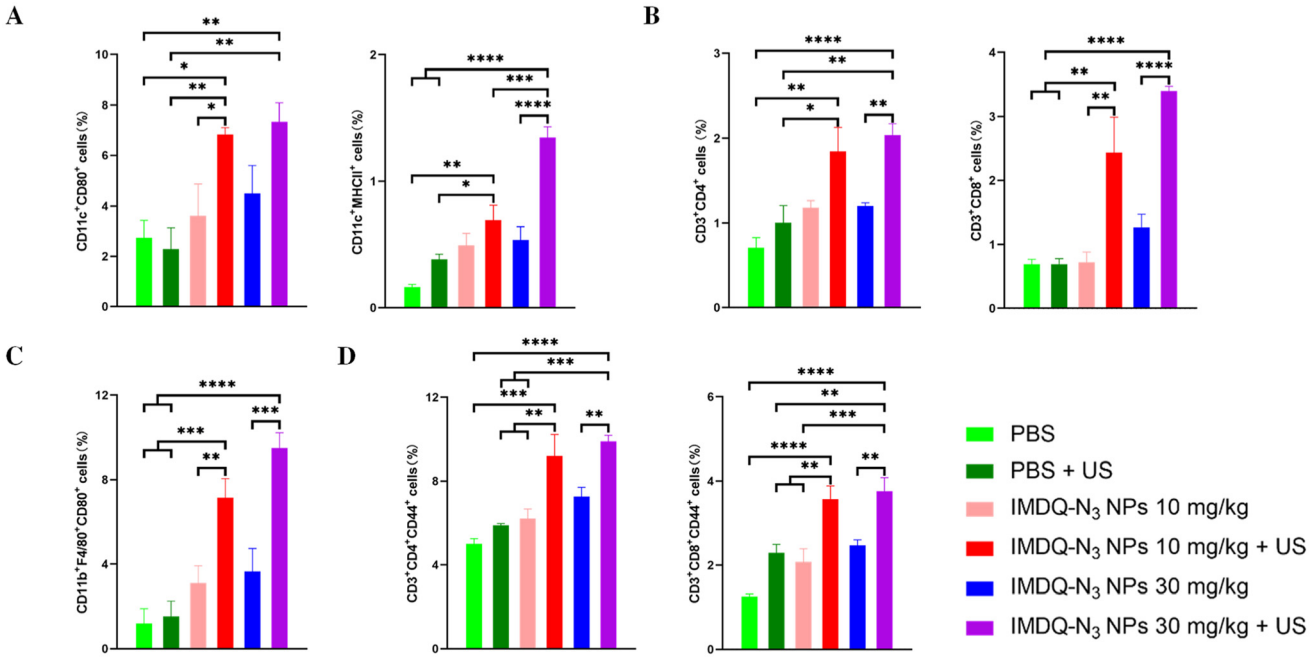

Fig. 5 Evaluation of immune-enhancing effect of IMDQ-N_3 NPs combined with US *in vivo*. (A) Flow cytometry analysis of DC activation in the tumor after treatment. (B) Flow cytometry analysis of $CD4^+$ T cells and $CD8^+$ T cells in the tumor after treatment. (C) Flow cytometry analysis of M1 macrophages in the tumor after treatment. (D) Flow cytometry analysis of immune memory cells in the spleen after treatment. Results are expressed as mean ± SEM (n = 4). P values were determined by one-way analysis of variance (ANOVA) followed by Tukey's Honestly Significant Difference test (*P < 0.05, **P < 0.01, ***P < 0.001 and ****P < 0.0001).

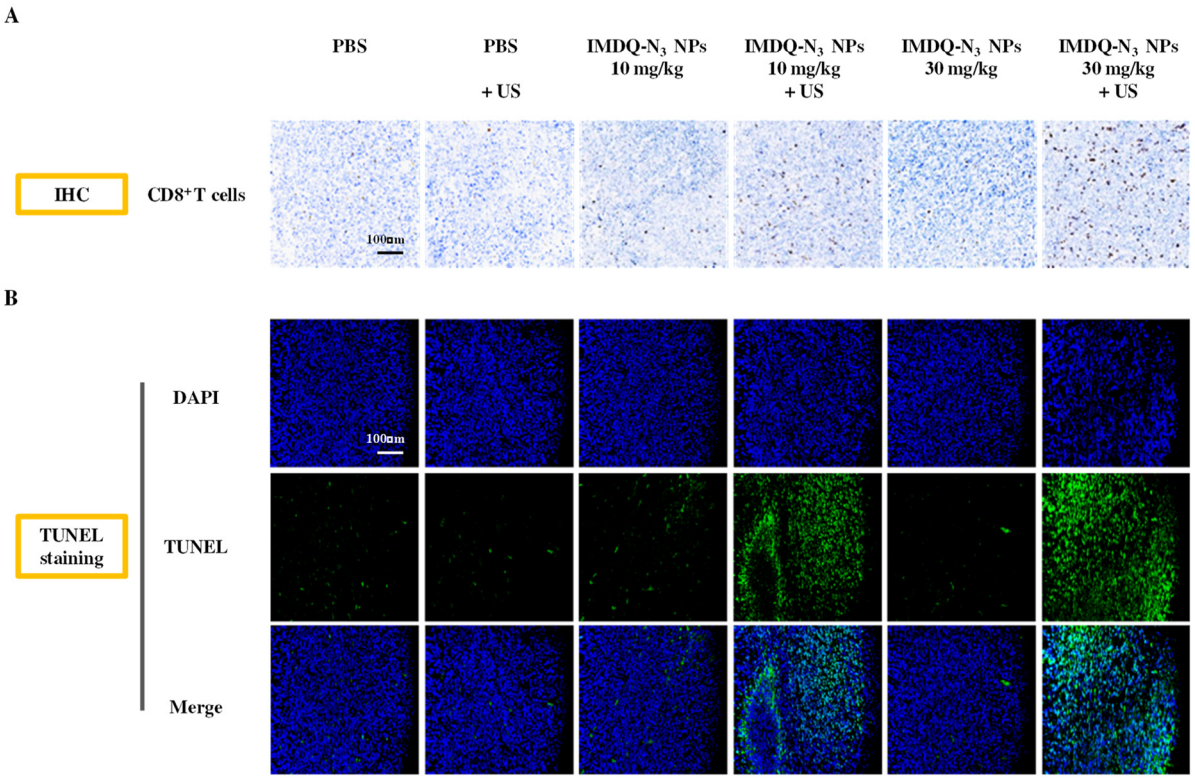

Fig. 6 (A) CD8 immunohistochemistry (IHC) staining of tumors after treatment. $CD8^+$ T cells are marked in gray. (B) TUNEL of tumors after treatment. Scale bar: 100 μm.

in treated mice. Throughout the treatment, the maximum body weight loss observed across all groups was 1.60% (Fig. 4D). Post-treatment analysis showed no significant differences in the serum levels of inflammatory cytokines, including IL-6, IFN-γ and tumor necrosis factor α (TNF-α), among all groups (Fig. 4E). Additionally, the survival time of CT26 tumor-bearing mice across different treatment groups was monitored. Notably, after 50 days, 60% of the mice treated with IMDQ-N_3 NPs and US remained alive, whereas all mice in the other groups succumbed within 31 days (Fig. 4F). Specifically, mice treated with PBS had a median survival time of 13 days, those treated with US alone had a median survival time of 15 days, and those treated with IMDQ-N_3 NPs alone exhibited a slightly extended median survival time of 19 days. These results further confirm the safety of IMDQ-N_3 NPs and demonstrate the efficacy of US-activated IMDQ-N_3 NPs in significantly inhibiting tumor growth.

The changes in the tumor immune microenvironment and splenic immune cells were monitored through flow cytometry after treatment (Fig. S8). Activated DCs ($CD11c^+CD80^+$ and $CD11c^+MHCII^+$) (Fig. 5A), T cells ($CD3^+CD4^+$ and $CD3^+CD8^+$) (Fig. 5B) and M1 macrophages ($CD11b^+F4/80^+CD80^+$) (Fig. 5C) in the tumor showed a significant increase overall. The immunohistochemical study of CD8 in the tumor also confirmed this (Fig. 6A). These results revealed that IMDQ-N_3 NPs activated by US could effectively heighten immunity in tumors. Furthermore, the obvious increase of different kinds of immune memory cells ($CD3^+CD4^+CD44^+$ and $CD3^+CD8^+CD44^+$) in the spleen showed that US-activated IMDQ-N_3 NPs effectively produced a lasting immunity (Fig. 5D).

The efficacy and safety were also demonstrated by several other evaluation methods. No obvious damage was observed by H&E staining and no significant hepatopulmonary metastasis except for the PBS group (Fig. S9) was observed. A higher apoptosis ratio of cancer cells was shown by TUNEL immunofluorescence staining in IMDQ-N_3 NPs with US groups (Fig. 6B). No evident changes of all groups in alanine aminotransferase (ALT), alkaline phosphatase (AKP), aspartate aminotransferase (AST), blood urea nitrogen (BUN), creatinine (CRE), and uric acid (UA) by blood chemical analysis, which showed no significant injury to the liver and kidney function (Fig. S10). All the results showed the high efficiency and low toxicity of US-sensitive IMDQ-N_3 NPs, which has revealed great potential in clinical tumor treatment.

4. Conclusions

To sum up, we have developed a novel, US-sensitive nanoprodrug, IMDQ-N_3 NPs, for tumor therapy and successfully mitigated the systemic toxicity of IMDQs. Both *in vitro* and *vivo*, IMDQ-N_3 NPs can be activated by US, resulting in the reduction of the prodrug to its active form, which exhibits immune-stimulating properties and promotes the maturation of APCs without being released from the polymer. The drug distribution in tissue experiment *in vivo* showed that the active drug could be restricted to the tumor rather than distributed throughout the body, effectively restraining the production of immune factor storms. IMDQ-N_3 NPs successfully inhibited the growth of the CT26 tumor, achieving a 95.7% tumor suppression rate and a survival rate of 60% on day 50 without evident side effects, under the activation of US. As a consequence, US-sensitive nano-prodrugs with non-cleavable linkers is a promising approach to tumor immunotherapy, providing a new feasible method for reducing the toxicity of immune-stimulating drugs.

Author contributions

C. L. and Y. Z. conducted the investigation. C. L., C. K., and Z. T. developed the concept. C. L. synthesized the samples, conducted the material characterization, analysed the data and wrote the paper. Y. X. and Z. T. provided important experimental insights. All the authors discussed the whole paper.

Conflicts of interest

There are no conflicts to declare.

Data availability

The data supporting this article have been included as part of the SI. The supplementary information contains the synthesis and characterization of constituent parts of nanoparticles; the pharmacokinetics, responsiveness, biodistribution and safety of IMDQ-N_3 NPs; and the gating strategy for flow cytometry. See DOI: **https://doi.org/10.1039/d5bm00755k**.

Acknowledgements

This work was supported by the National Natural Science Foundation of China (52403211, 52025035, 52495013), and Jilin Provincial International Cooperation Key Laboratory of Biomedical Polymers (YDZJ202402077CXJD).

References

1 Q. Lu, D. Q. Kou, S. H. Lou, M. Ashrafizadeh, A. R. Aref, I. Canadas, Y. Tian, X. J. Niu, Y. Z. Wang, P. Torabian, L. Z. Wang, G. Sethi, V. Tergaonkar, F. Tay, Z. N. Yuan and P. Han, *J. Hematol. Oncol.*, 2024, **17**, 48.
2 D. S. Chen and I. Mellman, *Immunity*, 2013, **39**, 1–10.
3 C. Lee-Chang and M. S. Lesniak, *J. Clin. Invest.*, 2023, **133**, 163449.
4 N. Bertho, B. Drénou, B. Laupeze, C. Le Berre, L. Amiot, J. M. Grosset, O. Fardel, D. Charron, N. Mooney and R. Fauchet, *J. Immunol.*, 2000, **164**, 2379–2385.
5 R. G. Everson, W. Hugo, L. Sun, J. Antonios, A. Lee, L. Z. Ding, M. L. S. Bu, S. Khattab, C. Chavez, E. Billingslea-

Yoon, A. Salazar, B. M. Ellingson, T. F. Cloughesy, L. M. Liau and R. M. Prins, *Nat. Commun.*, 2024, **15**, 13.
6 D. J. Dowling, *ImmunoHorizons*, 2018, **2**, 185–197.
7 J. Kim, S. Kang, J. Kim, S. B. Yong, S. F. Lahiji and Y. H. Kim, *Adv. Sci.*, 2024, **11**, 12.
8 M. Sanlorenzo, P. Novoszel, I. Vujic, T. Gastaldi, M. Hammer, O. Fari, C. D. Fernandes, A. D. Landau, B. V. Göcen-Oguz, M. Holcmann, B. Monshi, K. Rappersberger, A. Csiszar and M. Sibilia, *Nat. Cancer*, 2025, **6**, 42.
9 R. Li, L. Min, X. Wang, A. Chen, X. Chang, L. Cen, J. Chen, W. Sun, J. Yan, X. Zhou, J. Shen and B. Liu, *J. Clin. Oncol.*, 2023, **41**, 14666.
10 F. Janku, S.-W. Han, T. Doi, A. Amatu, J. A. Ajani, Y. Kuboki, A. Cortez, S. E. Cellitti, P. C. Mahling, K. Subramanian, H. A. Schoenfeld, S. M. Choi, L. A. Iaconis, L. H. Lee, M. R. Pelletier, G. Dranoff, V. Askoxylakis and S. Siena, *Cancer Immunol. Res.*, 2022, **10**, 1441–1461.
11 C. Rolfo, E. Giovannetti, P. Martinez, S. McCue and A. Naing, *npj Precis. Oncol.*, 2023, **7**, 26.
12 L. Nuhn, S. De Koker, S. Van Lint, Z. Zhong, J. P. Catani, F. Combes, K. Deswarte, Y. Li, B. N. Lambrecht, S. Lienenklaus, N. N. Sanders, S. A. David, J. Tavernier and B. G. De Geest, *Adv. Mater.*, 2018, **30**, 1803397.
13 S. Maddineni, M. Chen, F. Baik, V. Divi, J. B. Sunwoo and A. Finegersh, *Cancers*, 2023, **15**, 4386.
14 P. Li, C. Wang, H. Huo, C. Xu, H. Sun, X. Wang, L. Wang and L. Li, *Discover Nano*, 2024, **19**, 9.
15 L. Shi, S. Lin, F. Zhou, H. Jiang and J. Zhang, *Mater. Adv.*, 2024, **5**, 4634–4659.
16 Y. Xu, J. Lv, C. Kong, Y. Liu, K. Wang, Z. Tang and X. Chen, *Natl. Sci. Rev.*, 2024, **11**, 038.
17 E. Yoo, B. M. Crall, R. Balakrishna, S. S. Malladi, L. M. Fox, A. R. Hermanson and S. A. David, *Org. Biomol. Chem.*, 2013, **11**, 6526–6545.
18 N. M. Shukla, C. A. Mutz, S. S. Malladi, H. J. Warshakoon, R. Balakrishna and S. A. David, *J. Med. Chem.*, 2012, **55**, 1106–1116.
19 Z. Wang, Y. Gao, L. He, S. Sun, T. Xia, L. Hu, L. Yao, L. Wang, D. Li, H. Shi and X. Liao, *J. Med. Chem.*, 2021, **64**, 7507–7532.
20 Y. Xu, J. Lv, F. Liu, J. Wang, Y. Liu, C. Kong, Y. Li, N. Shen, Z. Gu, Z. Tang and X. Chen, *Adv. Mater.*, 2024, **36**, 2312493.
21 Y. F. Jiang, H. J. Chen, T. Lin, C. Zhang, J. X. Shen, J. F. Chen, Y. A. Zhao, W. Xu, G. W. Wang and P. T. Huang, *J. Nanobiotechnol.*, 2024, **22**, 12.
22 S. Glowniak, B. Szczesniak, J. Choma and M. Jaroniec, *Molecules*, 2023, **28**, 2639.
23 F. Foglietta, R. Canaparo, S. Cossari, P. Panzanelli, F. Dosio and L. Serpe, *Pharmaceutics*, 2022, **14**, 1102.
24 L. Tu, Z. Liao, Z. Luo, Y.-L. Wu, A. Herrmann and S. Huo, *Exploration*, 2021, **1**, 20210023.
25 Y. Q. Guo, Z. Q. Wang, G. M. Li, M. S. Zhan, T. T. Xiao, J. H. Wang, J. C. M. van Hest, X. Y. Shi and M. W. Shen, *Bioact. Mater.*, 2025, **43**, 129–144.
26 G. Liang, T. Sadhukhan, S. Banerjee, D. Tang, H. Zhang, M. Cui, N. Montesdeoca, J. Karges and H. Xiao, *Angew. Chem., Int. Ed.*, 2023, **62**, 202301074.
27 Y. D. Wang, H. D. Li, J. Y. Lin, Y. T. Li, K. Q. Zhang, H. Li, Q. Fu and Y. Y. Jiang, *Nat. Commun.*, 2025, **16**, 23.
28 P. L. Deena, S. J. Selvaraj and J. K. Thomas, *Orient. J. Chem.*, 2022, **38**, 1236–1243.
29 R. B. Silverman, G. R. Lawton, H. R. Ranaivo, L. K. Chico, J. Seo and D. M. Watterson, *Bioorg. Med. Chem.*, 2009, **17**, 7593–7605.
30 J. Geng, Y. Zhang, Q. Gao, K. Neumann, H. Dong, H. Porter, M. Potter, H. Ren, D. Argyle and M. Bradley, *Nat. Chem.*, 2021, **13**, 805–810.
31 X. Pan, L. Bai, H. Wang, Q. Wu, H. Wang, S. Liu, B. Xu, X. Shi and H. Liu, *Adv. Mater.*, 2018, **30**, 1800180.
32 N. Wang, L. Li, K. Wang, X. Huang, Y. Han, X. Ma, M. Wang, X. Lv and X. Bai, *Sustainability*, 2023, **15**, 15524.
33 Y. Xu, J. Chen, J. Ding, J. Sun, W. Song, Z. Tang and X. Chen, *Polym. Sci. Technol.*, 2025, **1**, 171–220.
34 J. Wu, *J. Pers. Med.*, 2021, **11**, 771.
35 J. He, Z. Liu, X. Zhu, H. Xia, H. Gao and J. Lu, *Pharmaceutics*, 2022, **14**, 1642.
36 G. Meng, T. Guo, T. Ma, J. Zhang, Y. Shen, K. B. Sharpless and J. Dong, *Nature*, 2019, **574**, 86–89.
37 H. Y. Yu, Z. H. Tang, M. Q. Li, W. T. Song, D. W. Zhang, Y. Zhang, Y. Yang, H. Sun, M. X. Deng and X. S. Chen, *J. Biomed. Nanotechnol.*, 2016, **12**, 69–78.
38 B. Chen, W. Dai, B. He, H. Zhang, X. Wang, Y. Wang and Q. Zhang, *Theranostics*, 2017, **7**, 538–558.
39 J. Liu, W. J. Tang, L. Chen, Q. Q. Zhang, T. Liu, L. Y. Qin, Y. M. Zhang and X. Chen, *Biomaterials*, 2025, **321**, 15.